

Electronic structure of Li-doped NiO

J. van Elp, H. Eskes, P. Kuiper, and G. A. Sawatzky

Department of Applied and Solid State Physics, Material Science Centre, University of Groningen, Nijenborgh 18, NL 9747AG Groningen, The Netherlands

(Received 29 May 1991)

The electronic structure of $\text{Li}_x\text{Ni}_{1-x}\text{O}$ has been investigated using x-ray photoemission spectroscopy (XPS), bremsstrahlung isochromat spectroscopy (BIS), and model-Hamiltonian cluster calculations. The measurements support the conclusion that the Li-doped holes have mainly oxygen character. The unoccupied electronic structure as probed with BIS shows broad structures growing in the gap. By comparing the XPS valence band to the results of the cluster calculations, we determine values for the Racah A parameter ($=6.6$ eV), charge transfer Δ ($=6.2$ eV), and hybridization transfer integral ($pd\sigma$) ($=1.3$ eV). The first ionization state in the NiO valence-band cluster calculation is of 2E_g symmetry, a state in which the doped hole is antiferromagnetically coupled to the Ni spins. Hole-doped cluster calculations explain, because of a different fractional parentage upon annihilating a Ni $3d$ or an O $2p$ hole, the difference between the O $1s$ XAS results and the BIS results of heavily Li-doped NiO.

INTRODUCTION

The electronic structure of the late-transition-metal monoxides has been a controversial subject for 40 years in which NiO has especially obtained a lot of attention because it is regarded as the prototype Mott-Hubbard¹⁻⁴ system. Since the discovery of the high- T_c superconductors,⁵ the interest in the late-transition-metal oxides, and especially the behavior on doping with holes, has been renewed. In the past, a wide range of doped late-transition-metal monoxide systems has been investigated.⁶ Based on magnetic measurements⁷ the charge compensating states in $\text{Li}_x\text{Ni}_{1-x}\text{O}$ were assumed to be of Ni^{3+} character, present in a low spin d^7 configuration. In a Mott-Hubbard system the strong d - d Coulomb interaction suppresses charge fluctuations like $d_i^n d_j^n \rightarrow d_i^{n+1} d_j^{n-1}$. A gap is opened with states of mainly $3d$ character on both sides of the gap. Substitutions of Li^{1+} for Ni^{2+} in NiO lead, in the Mott-Hubbard picture, to Ni^{3+} as the charge compensating state. These strong d - d Coulomb interactions are also the main reason for the breakdown of the one-electron picture.⁸

By using a configuration-interaction cluster model, Fujimori and Minami⁹ showed that the first ionization state of NiO is of mainly $d^8\bar{L}$ character (where \bar{L} denotes an oxygen hole), resulting in a ligand $2p$ to metal $3d$ gap. In this cluster calculation the mainly d^7 -like states are at higher binding energy and constitute the satellite. Evidence for this is found in resonant photoemission experiments¹⁰ where NiO shows strong resonances at higher binding energy.

This first ionization state of mainly $d^8\bar{L}$ character is of great importance for the character of the charge compensation states in $\text{Li}_x\text{Ni}_{1-x}\text{O}$ and suggests that this charge compensating state has mainly oxygen character. In an O $1s$ x-ray-absorption-spectroscopy (XAS) study Kuiper *et al.*¹¹ showed that the charge compensating holes for $\text{Li}_x\text{Ni}_{1-x}\text{O}$ are primarily on the oxygen and localized

around the Li impurity making it a semiconductor. Based on an analysis of various spectroscopies, they¹¹ also found a Ni-O antiferromagnetic exchange interaction two orders of magnitude larger than the superexchange interaction. The antiferromagnetic coupling of the oxygen hole spin with the Ni spin results in a static moment which looks like low spin Ni^{3+} ($S = \frac{1}{2}$). This antiferromagnetic coupling can in this way also explain the magnetic data.⁷

In this paper we present experimental [x-ray photoemission spectroscopy (XPS) and bremsstrahlung isochromat spectroscopy (BIS)] data on the $\text{Li}_x\text{Ni}_{1-x}\text{O}$ system. These measurements support the conclusion that the extra hole has substantial oxygen character. By using model-Hamiltonian cluster calculations we will reproduce the NiO valence band and we find that the first ionization state is of 2E_g symmetry. The extra hole in the first ionization state is also antiferromagnetically coupled. The unoccupied states as measured by BIS are found to be quite different from the O $1s$ XAS results. In contrast to a sharp impurity state in the gap as suggested by O $1s$ XAS we observe a broad band of states extending from about 0.5 eV above the top of the valence band all the way to the bottom of the d^9 conduction band of NiO. By using hole-doped cluster calculations this is explained as being a different fractional parentage in the electron addition spectral weight upon annihilating a Ni $3d$ hole as compared to an O $2p$ hole.

SAMPLE PREPARATION AND EXPERIMENTAL DETAILS

The $\text{Li}_x\text{Ni}_{1-x}\text{O}$ system is a room-temperature (RT) stable phase with possible Li substitution up to LiNiO_2 (Ref. 7) and beyond.¹² NiO has the NaCl structure¹³ which is slightly distorted below the Néel point at $T_N = 523$ K. Upon Li substitution it remains up to $x \sim 0.25$ in the NaCl structure; above this we have an or-

dering of the Li and Ni ions in (111) cation layers. In LiNiO_2 the cation layers are alternately occupied giving an enlarged Li-O distance, a shortened Ni-O distance,⁷ and the structure becomes hexagonal. The volume of the primitive cell decreases linearly with increasing Li content.⁷

The $\text{Li}_x\text{Ni}_{1-x}\text{O}$ samples are prepared by grinding together the proper proportions of Li_2CO_3 and NiO. The powders are mixed and pelletized and then heated at 950°C for more than 24 hours under a flow of dry oxygen. The x-ray diffraction data showed a homogeneous material but the method is not sensitive to the presence of unreacted Li_2O . The amount of Li put in is consistent with the lattice parameter variation as a function of the Li concentration,⁷ except for $x=0.4$, where the x-ray data gave $x=0.38$ indicating some unreacted Li_2O or Li volatilization.

The XPS and BIS measurements were performed using a modified Kratos 200 spectrometer, with a background pressure in the low 10^{-10} -mbar range. The XPS source was the unmonochromatized Al $K\alpha$ line (1486.6 eV). For BIS we use an Al $K\alpha$ (1486.6 eV) monochromator for photon detection and a home built type of Pierce electron gun, capable of giving electron currents of approximately 200 μA . The instrumental broadening is estimated to be 1.2 eV for XPS and 0.8 eV for BIS.

The higher-resolution XPS measurements on the 1% Li-doped NiO were performed using a commercially available X-Probe 300 spectrometer from Surface Science Instruments. The x-ray source is a monochromatized Al $K\alpha$ (1486.6 eV) line. The background pressure is in the low 10^{-10} -mbar range and the used experimental resolution is 0.9 eV.

All the ceramics reported here were glued to the sample holder with Ag epoxy glue and scraped *in situ* with a diamond file. To prevent the glue from degassing because of electrons heating the sample during the BIS measurements (150–300-mW heat load) we actually cooled down the sample holder to, for instance, -100°C . Although BIS measurements can be severely plagued by charging effects we encountered no charging effects except for the stoichiometric NiO sample, where BIS measurements were not possible. The necessary statistics in the BIS experiments were achieved by adding different scans with scraping in between. All the samples used for BIS measurements reported here were checked by XPS measurements before and after the BIS measurements.

EXPERIMENTAL RESULTS AND DISCUSSION

We start by comparing in Fig. 1 the O 1s core line of $\text{Li}_x\text{Ni}_{1-x}\text{O}$ with $x=0.2$ before and after the BIS measurements. We observe a peculiar effect in Fig. 1. The 530-eV high binding energy satellite of the O 1s core line which is mostly explained by assuming the presence of absorbed water, hydroxide, or defect structure at the surface actually decreases during the BIS measurements. By comparing the intensities of the O 1s and the Ni $2p_{3/2}$ core lines before and after BIS we find a decrease and not a shift of oxygen intensity toward the main line. To explain this we have to recall the way in which the ceramics

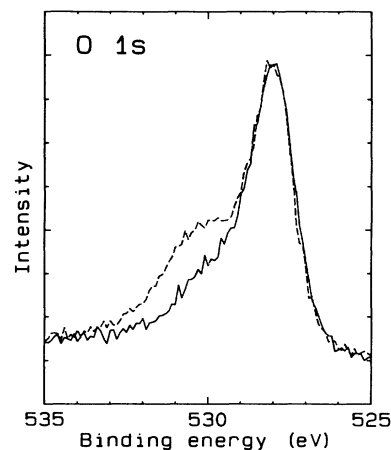


FIG. 1. Oxygen 1s core spectra of 20% Li-doped NiO before (dashed line) and after (solid line) the BIS experiment. The energy zero is the top of the valence band.

were made. The samples were, after heating, slowly cooled down to RT in an O_2 atmosphere. Defect structures of O_2^{2-} will probably form at the surfaces of the grain boundaries as is shown in a study on the defect structure of a NiO single crystal.¹⁴ In this study they created, through preferential sputtering, oxygen vacancies, and they studied the O 1s core line after oxygen exposure. A shoulder at high binding energy emerges, after high oxygen exposure, which they ascribe to O_2^{2-} at the oxygen vacancy. During electron bombardment in the BIS experiments this may break up, leaving O^{2-} at the oxygen vacancy, or even restoration of the local surface geometry. A short BIS measurement of only ten minutes was enough to get the intensity down; during the first ten minutes of measurements the pressure also went up. Scraping results in new fresh grain boundaries at the surface which again showed the same O 1s spectra before and after the BIS measurements.

In Fig. 2 we show the O 1s XPS core lines after the BIS measurements. There is still some intensity left at the high binding energy satellite which must be due to some absorbed water, hydroxide, or defect structure at the grain boundaries. Most important, however, is that we see no correlation between Li substitution and the intensity at the high binding energy satellite. The position of the O 1s core lines as compared to the top of the valence band changes from 528.4 eV in NiO to 528.0 eV for $x=0.4$ (see Table I).

The Ni $2p_{3/2}$ core line spectra as a function of the Li content are shown in Fig. 3. They consist of a main line at 854 eV and a satellite at 860 eV (labeled C). The NiO shows a double peaked main line (labeled A and B), and is comparable to the data of Hüfner and Wertheim.¹⁵ In the doped spectra we observe a narrowing of the main line and a loss of the double peaked structure. The satellite (C) exhibits, upon doping, a moderate decrease in intensity. The position of the onset of the Ni $2p_{3/2}$ core spectrum as measured halfway compared with the top of the valence band does not change with Li doping.

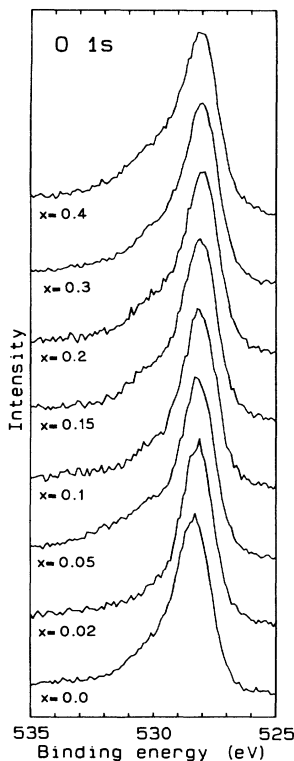


FIG. 2. Oxygen 1s core spectra of $\text{Li}_x\text{Ni}_{1-x}\text{O}$; the value of x is indicated in the figure. The energy zero is the top of the valence band.

The large satellite structure in the $\text{Ni } 2p_{3/2}$ core line of NiO has also been observed in the Ni dihalides¹⁶ and Cu dihalides¹⁷ and has been explained by use of cluster or impurity approximation model Hamiltonian calculations. In a simple approach the ground state of NiO is of the form

$$\psi_g = \alpha|d^8\rangle + \beta|d^9\bar{L}\rangle + \gamma|d^{10}\bar{L}^2\rangle, \quad (1)$$

where \bar{L} stands for an $\text{O } 2p$ hole. The ground state of Ni^{2+} in NiO is ${}^3A_{2g}$ (O_h symmetry) with two minority

TABLE I. $\text{O } 1s$ core line binding energy positions of $\text{Li}_x\text{Ni}_{1-x}\text{O}$. The energy reference is the top of the valence band. Except for NiO this is also the position of the Fermi level. In NiO the Fermi level is 1.2 eV in the gap, and the corresponding binding energy as compared to the Fermi level is 529.6 eV.

Composition	Energy (eV)
$x = 0$	528.4
$x = 0.02$	528.2
$x = 0.05$	528.1
$x = 0.1$	528.1
$x = 0.15$	528.1
$x = 0.2$	528.0
$x = 0.3$	528.0
$x = 0.4$	528.0

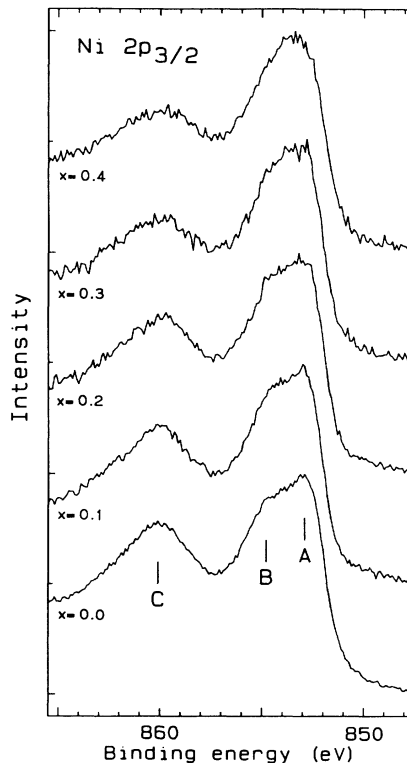


FIG. 3. The $\text{Ni } 2p_{3/2}$ core spectra of $\text{Li}_x\text{Ni}_{1-x}\text{O}$; the value of x is indicated in the figure. The labels A , B , and C are discussed in the text. The energy zero is the top of the valence band.

spin e_g holes. In the final states we have a Coulomb interaction Q between the created core hole (\bar{c}) and the $\text{Ni } 3d$ orbitals. The $\bar{c}d^9\bar{L}$ and $\bar{c}d^{10}\bar{L}^2$ are lowered by Q and $2Q$ as compared to $\bar{c}d^8$, this can result in a different ordering of the final-state levels, which is the reason for the strong satellite structure. In Fig. 4 we show the energy levels involved and the changes upon introducing the XPS core hole.

Taking into consideration the $\text{O } 1s$ XAS evidence for oxygen holes upon Li doping as the charge compensating states, one is tempted to expect satellite structure for $\text{Li}_x\text{Ni}_{1-x}\text{O}$ with high Li doping present at the $\text{O } 1s$ core line. A cluster calculation by Eskes and Sawatzky¹⁸ using

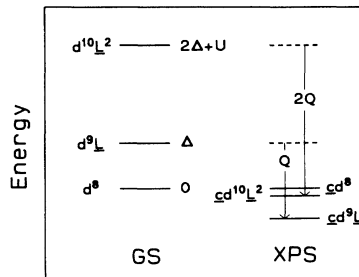


FIG. 4. Energy-level diagram of the ground state of NiO and the final states reached in the $\text{Ni } 2p$ core line XPS experiment.

a doped Cu_2O_7 cluster shows that very-low-intensity high binding energy satellites spread out over a wide energy range are present. We therefore expect to see even with O $2p$ holes present only one sharp O $1s$ core line.

The valence band of NiO and $\text{Li}_x\text{Ni}_{1-x}\text{O}$ for $x=0.4$ are shown in Fig. 5. In the $\text{Li}_x\text{Ni}_{1-x}\text{O}$ samples we find for $x \geq 0.02$ the Fermi level pinned at the top of the valence band. In NiO the Fermi level is 1.2 eV above the valence-band top and in Fig. 5 the spectrum is shifted over this energy to be able to compare it with the heavily doped one. We corrected the spectra for the x-ray Al $K\alpha_{3,4}$ satellites and carried out a background correction for inelastically scattered electrons. We assume that the background is proportional to the integrated intensity up to the top of the valence band. After this we normalized the two spectra to the O $2s$ core line intensity at 21-eV binding energy. Upon Li doping we find that there is an intensity decrease over the entire 10-eV spectral range, but with relatively little change in shape. The intensity decrease is expected because we have less Ni as compared to O. The XPS valence-band spectrum of NiO shows less structure at ~ 1 eV as compared to the XPS data of Hüfner and Wertheim¹⁵ or the UPS data of Oh *et al.*¹⁰, in which a 150-eV photon energy is used. In both, there is a shoulder at 2 eV which is not resolved in our data. In a high-resolution (0.9 eV) XPS measurement on a 1% Li-doped NiO we also find the shoulder at 2-eV binding energy (see Fig. 10 below).

The valence- and conduction-band spectral weight is almost completely determined by Ni $3d$ states. The cross-section ratio between Ni $3d$ and O $2p$ is ~ 25 ,¹⁹ so we see the Ni $3d$ states spread out over 10 eV because of the strong correlation effects. In the NiO XPS valence band a Coulomb interaction (U) between $3d$ holes raises the d^7 final state, which results in a different ordering and

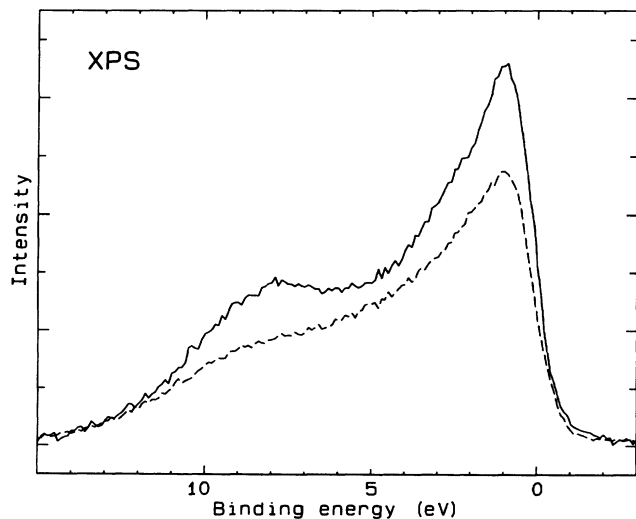


FIG. 5. The XPS valence-band spectra of NiO (solid line) and 40% Li-doped NiO (dashed line). The energy zero is the top of the valence band.

a spread of $3d$ spectral weight over 10 eV. In the cluster calculation below we will reproduce the XPS valence band of NiO and compare it with the high-resolution data of the 1% Li-doped NiO. The general conclusion we can draw from the XPS spectra is that upon Li substitution the local Ni electronic structure as probed by XPS is not much altered.

The BIS spectra shown in Fig. 6 however show a dramatic change upon Li substitution. The 2% Li-doped NiO shows a single d^9 peak with a small tail entering the gap. The spectrum is, except for the tail, the same as that published by Sawatzky and Allen,⁴ who also found a gap of ~ 4 eV and the maximum intensity of the d^9 state at 5.0 eV from the top of the valence band. Because we cannot determine the gap with an accuracy better than 0.3 eV, we have aligned the doped spectra at the d^9 -like state at 5.0 eV from the top of the valence band.

We see the Li induced impurity states growing in the gap extending from the foot of the d^9 peak at about 1 eV above the top of the valence band for $x=0.1$. At $x=0.4$ we find a sharp threshold in the BIS and only a small gap is left (~ 0.5 eV). The threshold is slowly moving to lower energy in going from $x=0.15$ to 0.4, thus increasing the distance between the edge of the Li induced states and the $d^9(\underline{L})$ -like state. At the same time there is a strong decrease in the spectral weight at 5.0 eV corresponding to the upper Hubbard band. Extrapolating to

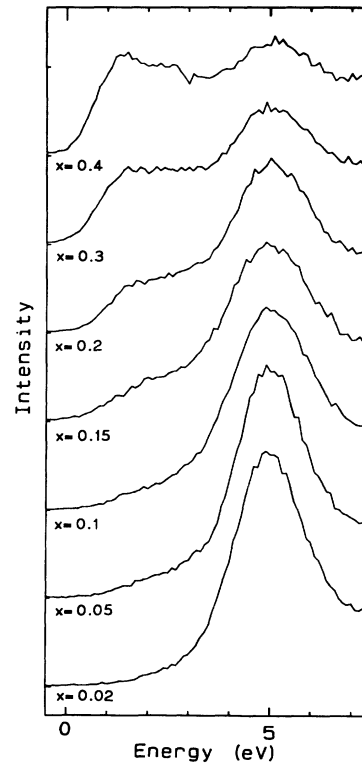


FIG. 6. The conduction-band spectra of $\text{Li}_x\text{Ni}_{1-x}\text{O}$; the value of x is indicated in the figure. The spectra are aligned on the d^9 conduction band peak of NiO at 5 eV. The energy zero is the top of the valence band.

LiNiO_2 we would expect that LiNiO_2 has little $d^9\bar{L}$ spectral weight left at 5.0 eV.

We can compare the BIS spectra with the O 1s XAS spectra published by Kuiper *et al.*¹¹ and shown in Fig. 7. In the O 1s XAS experiment the empty O 2p states are probed directly and the Ni 3d structure is seen because of the ground-state hybridization between Ni and O. The intensity of the Li induced states in the gap in the O 1s XAS experiment is much stronger than that found in the BIS experiment. This supports very strongly the conclusion already reached by Kuiper *et al.*¹¹ that the holes compensating the Li doping in $\text{Li}_x\text{Ni}_{1-x}\text{O}$ are of primarily O 2p character.

We analyzed the intensity in the BIS spectra and we show in Fig. 8 the difference spectra of $\text{Li}_x\text{Ni}_{1-x}\text{O}$ for $x > 0.02$ as compared to $x = 0.02$. We have assumed that the intensity increase of the Li induced impurity states is equal to the intensity loss of the d^9 -like state, so the area between -1 and 7.1 eV is taken to be constant. By calculating the area under the Li induced impurity states we find that the growth of the intensity of the Li impurity states is linear with the Li content. This linear increase of the impurity states upon doping is also found in the O 1s XAS results.¹¹ The difference spectra show even for low Li doping a broad structure growing in the gap. For $x = 0.05$ the growth of the induced impurity states is

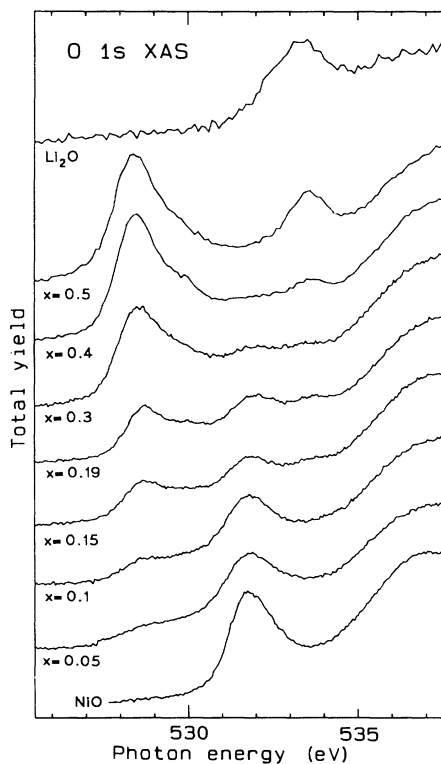


FIG. 7. The oxygen 1s absorption spectra of $\text{Li}_x\text{Ni}_{1-x}\text{O}$ as published by Kuiper *et al.*¹¹ The value of x is indicated in the figure. The intensity increase at 533.5-eV photon energy for $x = 0.4$ and 0.5 is a result of unreacted Li_2O present in the samples.

spread over 2 eV. These broad structures are also seen with increasing Sr doping in the conduction band of $\text{La}_{2-x}\text{Sr}_x\text{NiO}_4$,^{20,21} where the gap is eventually closed upon high doping and conductivity measurements show metallic behavior.^{22,23} The $\text{Li}_x\text{Ni}_{1-x}\text{O}$ system shows semiconducting behavior up to high Li substitution. This is explained by Kuiper *et al.*¹¹ by the influence of the Li impurity potential, localizing the introduced O 2p holes even up to high-Li-doping concentrations.

OXYGEN HOLE SYMMETRY CALCULATIONS

As suggested by Kuiper *et al.*¹¹ it is possible that the extra hole is actually localized around the Li impurity. The Li^{1+} in the lattice can be written as $(\text{Li}^{2+})^{1-}$, and the Li impurity therefore has, relative to the lattice, an attractive potential for holes. If the hole around the Li is delocalized over four to six oxygen neighbors the symmetry and energetics of such a localized hole can be investigated if we consider a $(\text{Li})\text{O}_6$ cluster in O_h symmetry. The O_6 cluster has a total of 18 $p_{\alpha,i}$ orbitals (with p_α being p_x , p_y , or p_z and i the position in the cluster $i \in [1, 6]$). These 18 O 2p orbitals are split in the following O_h symmetry orbital combinations: one A_{1g} , two E_g , three T_{1g} , three T_{2g} , three T_{2u} , and six T_{1u} orbitals. The energies of these oxygen hole symmetries are determined by the nearest-neighbor oxygen interactions as written in terms of Slater-Koster²⁴ two-center transfer integrals ($pp\sigma$) and ($pp\pi$). The energies of these different sym-

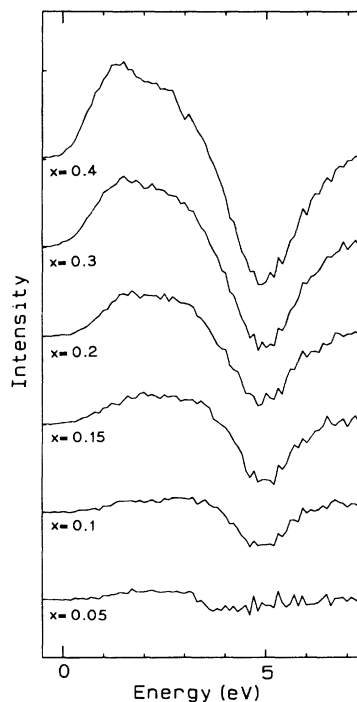


FIG. 8. The change of unoccupied electronic structure upon Li doping of NiO. The reference spectrum is the 2% Li-doped NiO, and the difference spectra of $\text{Li}_x\text{Ni}_{1-x}\text{O}$ are shown for $x = 0.05$ to 0.4 . The energy zero is the top of the valence band.

TABLE II. Oxygen hole symmetry calculations on O_h symmetry using an O_6 cluster.

Symmetry	Energy ($(pp\sigma), (pp\pi)$)	Energy (eV)
A_{1g}	$-2(pp\sigma) + 2(pp\pi)$	1.40
E_g	$(pp\sigma) - (pp\pi)$	-0.70
T_{1g}	$(pp\sigma) - (pp\pi)$	-0.70
T_{2g}	$-(pp\sigma) + (pp\pi)$	0.70
T_{2u}	$-2(pp\pi)$	-0.30
T_{1u}	$(pp\pi) + \sqrt{[(pp\pi)^2 + 2(pp\sigma) + (pp\pi)]^2}$	0.73
T_{1u}	$(pp\pi) - \sqrt{[(pp\pi)^2 + 2(pp\sigma) + (pp\pi)]^2}$	-0.43

metries are given in Table II. The lowest energy for a hole is found by taking $(pp\sigma) < 0$, $(pp\pi) > 0$, and $(pp\pi) \sim -0.3(pp\sigma)$ which is a relation also found in tight-binding calculations of transition-metal oxides.²⁵ The lowest-energy states are of E_g and T_{1g} symmetry contrary to the A_{1g} symmetry suggested by Kuiper *et al.*¹¹. The Li impurity potential will split these symmetries further, because the E_g symmetry consists of a combination of σ -bonding orbitals with lobes pointing toward the Li impurity in contrast to the π -bonding orbital combinations of T_{1g} symmetry. The attractive Li impurity potential will lower the E_g symmetry orbitals.

We can compare the results of the calculation with one hole in the O_6 cluster with the results of a fcc oxygen lattice linear combination of atomic orbitals tight-binding calculation. In this calculation also only the nearest-neighbor oxygen interaction transfer integrals $(pp\sigma)$ and $(pp\pi)$ are used. Every k point can be projected onto orbital combinations belonging to the different symmetries of O_h found in the cluster calculation. The density of states for a hole in every symmetry can be found. The results are shown in Fig. 9 for $(pp\sigma) = -0.55$ eV and $(pp\pi) = 0.15$ eV. These values of $(pp\sigma)$ and $(pp\pi)$ result in a total oxygen bandwidth of ~ 4 eV, a value which is observed in the late-transition-metal oxides.²⁶ In Fig. 9 we also indicated the energy positions of the cluster calculation as vertical solid lines.

The E_g symmetry oxygen holes have the same symmetry as the $3d$ orbitals $d_{x^2-y^2}$ and $d_{3z^2-r^2}$. In systems in which we have one hole in the double degenerate transition-metal $3d$ e_g symmetry orbitals, for instance, Cu^{2+} , this leads to a Jahn-Teller distortion and a splitting of the degeneracy. It is however not clear if such a splitting and lattice distortion for two E_g symmetry oxygen hole combinations actually occurs. In these calculations we assumed that the hole is delocalized on four to six oxygens. Hartree-Fock molecular cluster calculations^{27,28} however suggest that a hole around a Li impurity is localized on one neighboring oxygen, leading to a local symmetry of C_{4v} and an electric dipole. Evidence that the Li impurity in NiO has an electric dipole moment also comes from dielectric loss measurements.^{6,29}

MODEL HAMILTONIAN CLUSTER CALCULATIONS

To determine values for the various interactions discussed above and to investigate the doping behavior

theoretically we compare the experimental spectra to the results of cluster calculations. The aim of the cluster calculation is to obtain (a) the Ni $3d$ electron removal spectral weight, to be compared with the Ni valence-band XPS, (b) the character (symmetry, spin, and orbital composition) of the first ionization state of NiO, and (c) the electron addition spectral weight of hole-doped NiO. The model calculations use a NiO_6 cluster in octahedral symmetry. The model Hamiltonian is given by

$$H = H_0 + H_1, \quad (2)$$

$$H_0 = \sum_m E_d(m) d_m^\dagger d_m + \sum_m E_p(m) p_m^\dagger p_m + \sum_m T_{pd}(m) (d_m^\dagger p_m + p_m^\dagger d_m), \quad (3)$$

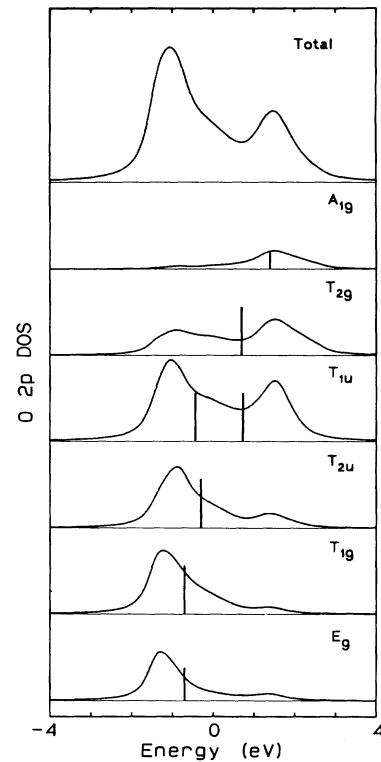


FIG. 9. The oxygen $2p$ dos in a tight binding calculation of a fcc oxygen lattice. The negative energy indicates the lowest energy of the oxygen hole. The oxygen $2p$ dos is projected on different O_h symmetries. The vertical bars indicate the energy positions of these O_h symmetries in an O_6 cluster calculation.

$$H_1 = \sum_{m,m',n,n'} U(m,m',n,n') d_m^\dagger d_m d_n^\dagger d_n. \quad (4)$$

The indices m , m' , n , and n' denote orbital and spin quantum numbers. We include all the Ni $3d$ orbitals, but only the oxygen orbital combinations which can hybridize with the Ni $3d$ orbitals. As a "vacuum" for NiO we take the Ni^{2+} (d^8) Hund's-rule ground state (${}^3A_{2g}$ in O_h symmetry with two e_g holes) and a closed oxygen $2p$ shell. The operator d_m^\dagger creates a Ni $3d$ hole with energy $E_d(m)$. We have included a point charge crystal field splitting ($10Dq$), which splits the $3d$ orbital energies in a double degenerate e_g level at $E_d(e_g) = E_d - 6Dq$ and a triple degenerate t_{2g} level at $E_d(t_{2g}) = E_d + 4Dq$. The value used in NiO for $10Dq$ ($10Dq = 0.7$ eV) is equal to a value found in an impurity calculation³⁰ of the optical spectrum of NiO and is consistent with the experimental data.

The operator p_m^\dagger creates an O $2p$ hole with energy $E_p(m)$. The ligand hole wave functions consist of linear combinations of oxygen $2p$ orbitals with the appropriate (d orbital) symmetries. As discussed above, the Slater-Koster²⁴ oxygen nearest-neighbor interactions ($pp\sigma$) and ($pp\pi$) split the oxygen states into a double degenerate state with e_g symmetry at $E_p(e_g) = E_p + ((pp\sigma) - (pp\pi))$ and a triple degenerate state with t_{2g} symmetry at $E_p(t_{2g}) = E_p - ((pp\sigma) - (pp\pi))$. The value of $(pp\sigma) - (pp\pi)$ for NiO is governed by the width of the oxygen band in NiO (~ 4 eV) and is consistent with band-structure calculations and photon-dependent normal emission experiments on a single crystal of NiO.²⁶

The last term of H_0 describes the one-particle hybridization between the Ni $3d$ states and the ligand orbitals. T_{pd} is the transfer integral for Ni $3d$ –O $2p$ hybridization. This is written in terms of Slater-Koster²⁴ ($pd\sigma$) and ($pd\pi$) transfer integrals. We define Δ as the energy needed in the ground state for removing an electron from the O $2p$ occupied states to a Ni $3d$ empty state ($\Delta = E_p - E_d$).

H_1 describes the two-particle $3d$ Coulomb and exchange interactions U . The calculation includes the d - d Coulomb and exchange interactions using the full atomic multiplet theory as specified in terms of the Racah A , B , and C parameters. For NiO the B and C parameters of the unscreened atomic values of Ni^{2+} are taken as tabulated by Griffith.³¹

In this Hamiltonian we have neglected the Ni $4s, 4p$ levels and the empty O bands. These levels are assumed to be at high energy so that their influence through hybridization can be treated as a renormalization of the effective parameters. We also neglect the O-O Coulomb interaction. The many-body Hamiltonian is solved exactly by means of a continued fraction expansion of the Green's function giving directly the electron removal or addition spectra.

For the actual calculation of the NiO $3d$ removal spectral weight we treat three parameters as free variables. These are the charge-transfer energy Δ , the Racah A parameter responsible for the d - d Coulomb interaction and the Ni-O transfer integral ($pd\sigma$). The transfer integral ($pd\pi$) is taken to be $-0.45(pd\sigma)$.³² The parameters for the NiO electron removal spectral weight are obtained

from the experimental data with the following criteria: (a) the spectral weight must be spread over 10 eV, (b) the intensity around 8-eV binding energy must be about 30% of the intensity in the main line and the shoulder, and (c) a gap of about 5 eV must exist, which is larger than the experimental value to take the translational invariance into account.

In Fig. 10 we show the fit and the high-resolution experimental data of 1% Li-doped NiO and in Table III we list our parameters used. We have found no reasonable parameter set which produces the correct intensity for the shoulder at 2-eV binding energy (labeled B in Fig. 10) and the spread in the high binding energy satellite (labeled C). So we reproduced the intensity difference between the main line (A) and shoulder (B) as compared to the satellite (C). The high binding energy satellite (C) is more spread out in the experiment. This could be due to lifetime effects or because these states hybridize with the $d^9\bar{L}^2$ final states present at this position which are spread out considerably because of the ligand hole band. In an impurity calculation by Zaanen,³⁰ in which the O $2p$ bandwidth is fully taken into account, the spectral weight at this high binding energy (C) is spread out much stronger. Photoemission from the O $2p$ orbitals is about 4% of the Ni $3d$ spectral weight; one can take this into account by adding 4% O $2p$ spectral weight around 4 ± 2 eV. Taking these considerations into account the fit is reasonable. We find a calculated gap of 5.0 eV. The electron addition spectral weight is characterized by one state of mainly d^9 character (97% d^9) as expected and one mainly $d^{10}\bar{L}$ final state at $A + \Delta$.

In Fig. 11 we show the electron removal spectral weight for changes in the parameter set. A smaller hybridization ($(pd\sigma) = 1.0$ eV) reduces the spread in spectral weight and increases the spectral weight at higher binding energy. This indicates that we are in the charge-transfer regime, because with a smaller hybridization spectral weight will be transferred from the $d^n\bar{L}$ states to the d^{n-1} states. increasing the Racah A parameter as compared to Δ increases the intensity at higher binding energy and also results in a small increase in spread of the spectral weight. All three parameters determine the in-

TABLE III. The model parameter values used in the NiO_6 cluster calculation. Energies are in eV.

Parameter	Value
Racah A	6.6
Racah B	0.13
Racah C	0.60
Δ	6.2
$(pd\sigma)$	1.3
$(pd\pi)$	-0.6
$(pp\sigma)$	-0.55
$(pp\pi)$	0.15
$10Dq$	0.7
$U({}^4T_{1g})$	6.7
$U({}^2E_g)$	10.0
E_{gap}	5.0

tensity slope and the spread in spectral weight. The gap is mainly determined by A and Δ .

In Fig. 10 we also show the different final-state symmetries and their spectral weights. The 4E_g final state can only be reached because of hybridization in the ground state and its intensity is a result of the removal of the charge-transferred ninth d electron of $d^9\bar{L}$. This final state is of mainly $d^8\bar{L}$ character because it cannot hybridize with a d^7 final state. In Table IV we list the amount of $d^7, d^8\bar{L}$ etc. present in the first ionization states.

The first ionization state is of 2E_g symmetry, a state in which the extra hole has the $3d e_g$ majority spin symmetry, and the $d^8\bar{L}$ component has the strongest contribution indicating that the extra hole has gone mainly on oxygen (\bar{L}). The second ionization state is the ${}^4T_{1g}$ high-spin state. This first ionization state of 2E_g character is not found as the first ionization state in the cluster calculation of Fujimori and Minami.⁹ They find a ${}^4T_{1g}$ symmetry state as the first ionization state and basically the first states (${}^4T_{1g}, {}^2E_g$, and ${}^2T_{1g}$) in the same order as in a ligand field interpretation.³³ The impurity calculation of Zaanen³⁰ shows both 2E_g and ${}^4T_{1g}$ spectral weights as first ionization states. This is most likely a result of the use of a smaller ionic contribution to the ligand field

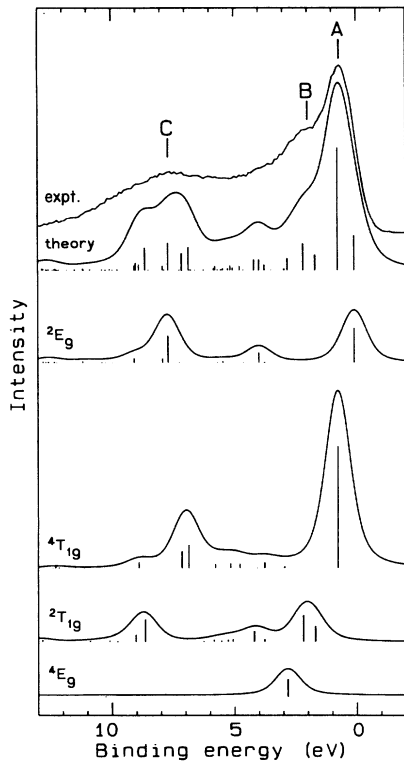


FIG. 10. The XPS valence-band spectrum (top, experiment of 1% Li-doped NiO compared to the electron removal spectral weight of the cluster calculation (top, theory). The vertical bars indicate the position and intensity of the final states. In the bottom we show the electron removal spectral weight for the different final-state symmetries (${}^2E_g, {}^4T_{1g}, {}^2T_{1g}$, and 4E_g). The energy zero is the top of the valence band.

TABLE IV. Occupation numbers of the ground state and first two ionization states of NiO.

Ground state		Ionization states		
		2E_g	${}^4T_{1g}$	
d^8	0.819	d^7	0.171	0.324
$d^9\bar{L}$	0.176	$d^8\bar{L}$	0.659	0.583
$d^{10}\bar{L}^2$	0.005	$d^9\bar{L}^2$	0.164	0.091
		$d^{10}\bar{L}^3$	0.006	0.002

splitting ($10Dq=0.4$ eV) and the use of a single O $2p$ density of states instead of different O_h symmetry O $2p$ density of states. The difference between the E_g and T_{2g} symmetry projected density of states in the ligand band is considerable as shown above. In our oxygen cluster calculation this O $2p$ splitting results in ligand hole states which are $2((pp\sigma)-(pp\pi))$ apart with the E_g as the lowest one. This has a large effect on the first ionization state, because $U \sim \Delta$.

By using the same model Hamiltonian and the parameters obtained by comparing the NiO valence-band spectrum to the $3d$ electron removal spectral weight we can also calculate the energies of the $d-d$ optical transitions from the ground state of NiO. In Table V we compare our calculated values with the experimental $d-d$ optical

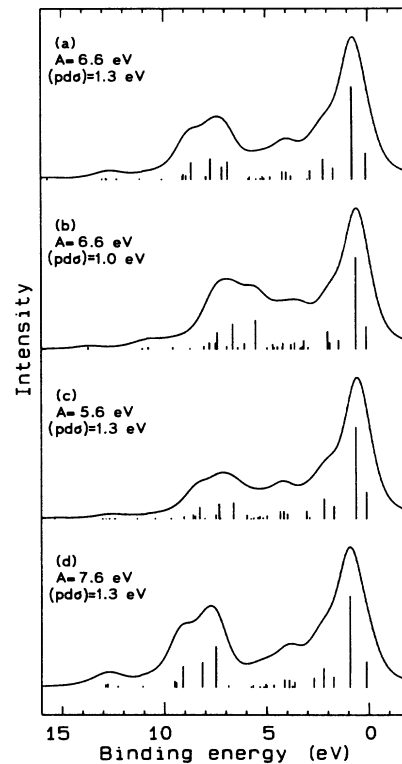


FIG. 11. The effect of different parameters on the $3d$ electron removal spectral weight. (a) The standard parameter set of Table III. (b) $pd\sigma=1.0$ eV instead of 1.3 eV. (c) and (d) Change of the Racah A parameter. $A=5.6$ eV (c) and $A=7.6$ eV (d).

TABLE V. Energy and symmetry of the calculated $d-d$ optical forbidden absorptions in NiO using the parameters of Table III. The values of the experimental absorption energies as measured by Newman and Chrenko² are also listed. Energies are given in eV.

Energy position		Symmetry
Theory	Experiment	
1.22	1.13	${}^3T_{2g}$
1.68	1.75	1E_g
1.98	1.95	${}^3T_{1g}$
2.64	2.75	${}^1A_{1g}$
3.00	2.95	${}^1T_{2g}$
3.37	3.25	${}^3T_{1g}$
3.49	3.52	${}^1T_{1g}$

absorption energies as measured by Newman and Chrenko.³⁴ The agreement is within 0.1 eV for all energy positions calculated which is quite good. The energy of the first $d-d$ optical transition (${}^3A_{2g} \rightarrow {}^3T_{2g}$) has always been identified as the ligand field splitting between $3d e_g$ and t_{2g} orbitals. Its value is larger than the included point charge crystal field splitting ($10Dq$). This is a result of the different hybridization contributions to the ${}^3A_{2g}$ ground state and the ${}^3T_{2g}$ excited state. This agreement is a strong confirmation for the value taken for the point charge crystal field splitting ($10Dq = 0.7$ eV).

To determine in what region of the Zaanen, Sawatzky, and Allen³⁵ (ZSA) classification scheme NiO should be placed we have to compare U with Δ . If we determine U from the lowest free ion multiplets of d^7 , d^8 , and d^9 we find $U({}^4T_{1g}) = A + B = 6.7$ eV. Compared with $\Delta = 6.2$ eV this would place NiO in the intermediate region of the ZSA (Ref. 35) diagram. If however we have a critical look at the character of the first ionization state (Table IV) we find much more $d^8\bar{L}$ character than d^7 character. The U determined above is the U belonging to the ionization state of ${}^4T_{1g}$ symmetry, which is not the first ionization state found. The U belonging to the first ionization state has a value $U({}^2E_g) = 10.0$ eV, much larger than Δ . So we would like to place NiO in the charge-transfer regime of the ZSA phase diagram.³⁵

In the $\text{Li}_x\text{Ni}_{1-x}\text{O}$ system the Li substitution can go up to $x = 0.5$ continuously, along with a continuous change in electronic structure as shown above. It is therefore useful to look at the results of a hole-doped NiO cluster calculation. We use the same parameters as determined for NiO and assumed that the parameters obtained are still valid for LiNiO_2 with, however, three holes in the ground state instead of two. As stated above we neglect the oxygen $2p-2p$ Coulomb interactions, which might, because of the considerable amount of \bar{L}^2 state present, not be valid any more. Even more important is that we assume that the extra doped hole in LiNiO_2 is localized around the Ni instead of around a Li as is suggested by Kuiper *et al.*,¹¹ or localized on one oxygen around a Li.^{27,28} The structure of LiNiO_2 is such that a hole in a σ -bonding oxygen near a Li automatically has a Ni on

the other side. So a hole near a Li is, in LiNiO_2 , also near a Ni. In the calculations, however, the \bar{L} states are delocalized over four to six oxygen neighbors with appropriate phase factors. If the hole is localized on one single oxygen the phase coherence is lost. This leads to a lower transfer integral. Instead of $\sqrt{3}(pd\sigma)$ we have $\sqrt{3}/2(pd\sigma)$ for the σ -bonding oxygen hole and $(pd\pi)$ instead of $2(pd\pi)$ for the π -bonding oxygen. The ground-state occupation will change because of this different hybridization. The energy positions of the electron addition final states will not change much because they depend most strongly on $10Dq$ and the Racah B and C parameters. The intensity however can change. The results of the cluster calculation on the electronic structure of LiNiO_2 can be compared with the experimental data for $x = 0.4$.

Using the parameters of NiO we find that in LiNiO_2 the $d^8\bar{L}$ level is below the d^7 level which is a direct result of $U > \Delta$ in NiO. So in defining a new Δ for LiNiO_2 one would find that Δ is negative.

In the $3d$ electron addition spectral weight (see Fig. 12) for the hole-doped 2E_g ground state we find the three strongest final states spread out over 3 eV. These states are of mainly d^8 character with ${}^3A_{2g}$, 1E_g , and ${}^1A_{1g}$ symmetry. The intensity of these three states is roughly expected to be equal because the ground state has $(e_g\uparrow)^2(e_g\downarrow)$ holes (for a part on Ni or in the O $2p$ orbitals). This results in a ${}^3A_{2g}$ first electron addition (BIS) final state by filling up the $(e_g\downarrow)$ and in higher-energy final states of 1E_g and ${}^1A_{1g}$ symmetries through filling up an $(e_g\uparrow)$. The final states at about 6-eV higher energy are mainly of $d^9\bar{L}$ character. The broad structures growing in the gap observed in the BIS data upon Li doping is explained as being a result of different multiplets reached upon electron addition. The gap between the first electron removal and first electron addition final states in the cluster calculation has disappeared for the hole-doped 2E_g ground state. The actual gap in the highly doped $\text{Li}_x\text{Ni}_{1-x}\text{O}$ is of the order of 0.5 eV and is most likely a result of a potential localizing the doped oxygen holes,

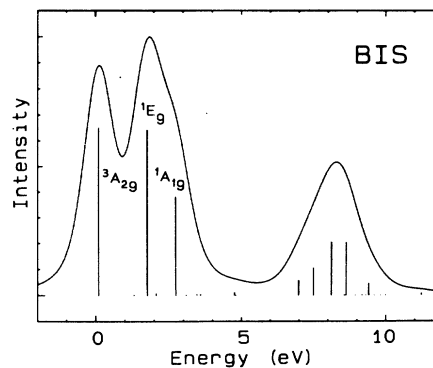


FIG. 12. The calculated $3d$ electron addition spectral weight of the hole-doped 2E_g ground state. The symmetry of the strongest three mainly d^8 final states is shown.

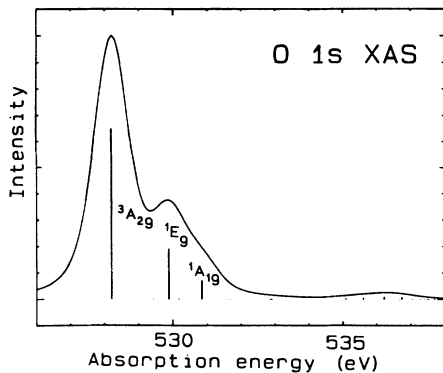


FIG. 13. The calculated O $2p$ electron addition spectral weight of the hole-doped 2E_g ground state. The symmetry of the strongest three mainly d^8 final states is shown. The energy scale of the spectrum is shifted to the O $1s$ absorption energy of the highly Li-doped NiO spectra.

and/or of a Coulomb interaction between the O $2p$ holes.

To explain the different spectral weight in the O $1s$ XAS spectra for high Li doping as compared with the BIS spectra we determined the electron addition spectral weight for adding an electron explicitly to the symmetrized oxygen $2p$ orbitals. In this way we take the different ground-state occupations of $d^8\bar{L}$ into account, which influences the final-state spectral weights strongly because of the optical selection rule in which the main absorption process is $d^8\bar{L} \rightarrow \underline{c}d^8$. We neglect the influence of the oxygen core hole (\underline{c}) because if we have a pure $\underline{c}d^8$ final state the core hole is on an oxygen and the extra $3d$ added electron is on the Ni ion, well separated from each other. The first electron addition final states have an additional $d^9\bar{L}$ contribution, so that a core hole can influence the result somewhat. We show the results in Fig. 13. We find the same three symmetry final states (respectively, ${}^3A_{2g}$, 1E_g , and ${}^1A_{1g}$) as seen in the BIS but the intensity distribution is very different. The mainly $\underline{c}d^9\bar{L}$ final states at about 6-eV higher energy have little intensity left. To understand the asymmetric intensity distribution we must inspect the orbital composition of $d^8\bar{L}$ in the 2E_g ground state. We have 65.9% $d^8\bar{L}$ character, which is split in $d^8\bar{L}$ of $(e_g \uparrow)^2(\bar{L}(e_g \downarrow))$ character with 34.1%, $(e_g \uparrow)(\bar{L}(e_g \uparrow))(e_g \downarrow)$ character with 29.7%, and the remaining 2.1% consists of $(t_{2g})^2(\bar{L}(t_{2g}))$ combinations of 2E_g symmetry mixed in the ground state. The ${}^3A_{2g}$ symmetry final state is reached by filling up the ligand hole in $(e_g \uparrow)^2(\bar{L}(e_g \downarrow))$. These different orbital compositions present in the doped ground state explain the much stronger intensity of the ${}^3A_{2g}$ $\underline{c}d^8$ final state reached in the O $1s$ XAS. The different shape in the O $1s$ XAS as compared with the BIS is a direct result of the different fractional parentage found in annihilating a Ni $3d$ hole as compared to an O $2p$ hole.

Although the doped ground-state (2E_g) symmetry in the calculations is different from what we expect (hole around Li instead of Ni), the general explanation for the

BIS and the difference between BIS and O $1s$ XAS will not change. Experimentally the added hole is coupled antiferromagnetically, resulting in low-spin “ Ni^{3+} .” But here also the two original holes of the Ni can change through Li doping to ${}^1A_{1g}$ and 1E_g symmetries. So the general picture stays unchanged.

In the O $1s$ XAS data for $x=0.4$ a small shoulder at higher absorption energy is observed (see Fig. 7). The $\underline{c}d^9\bar{L}$ final state is for $x=0.4$ decreased to negligible intensity. The structure coming up at 533.5-eV absorption energy is a result of unreacted Li_2O present as can be deduced from the Li_2O O $1s$ XAS spectrum.

Kuiper *et al.*¹¹ suggested that the sharp structure seen in the O $1s$ XAS spectrum is due to O $2p$ states split off from the O $2p$ band because of the Li impurity potential. From the BIS measurements however we find spectral weight extending over the whole gap region. The difference between BIS and XAS could then be due to the influence of the core hole in XAS. However, we have shown that the spectral weight in the gap in BIS probably is due to multiplet structure rather than banding. The sharper structure seen in XAS can then be explained by different fractional parentage due to different selection rules. These broad structures seen in the gap are completely different than those found in a similar study on the $\text{Li}_x\text{Co}_{1-x}\text{O}$ system³⁶ in which the gap stays open up to the highest possible Li substitution ($x=0.2$) and the Fermi level is pinned in the gap.

CONCLUSIONS

We have presented spectroscopic data on $\text{Li}_x\text{Ni}_{1-x}\text{O}$. The XPS data show that upon Li addition the local Ni electronic structure as probed by XPS is not much altered. The BIS data show a dramatic change upon Li substitution and, by comparing it with the O $1s$ XAS data, we find that the holes compensating the Li^{1+} charge in $\text{Li}_x\text{Ni}_{1-x}\text{O}$ are of mainly oxygen character. In contrast to the O $1s$ spectra we observe in the BIS spectra a broad structure growing in the gap. By using a model cluster calculation we find model parameters describing the electronic structure of NiO. The first ionization state is of 2E_g character. On doping with holes this is expected to be the charge compensating state and the magnetic moment of this charge compensating state looks macroscopically like Ni^{3+} in low spin ($S=\frac{1}{2}$). Calculations using the hole-doped 2E_g symmetry state as the ground state explains the difference observed in the unoccupied states as probed with O $1s$ XAS or BIS. A different fractional parentage upon annihilating a Ni $3d$ or O $2p$ hole is most likely responsible for the sharp feature seen in the O $1s$ XAS experiment. For low Li doping the hole will be localized around a Li impurity in a mainly oxygen orbital combination of E_g symmetry if we do not allow for a local distortion to lower symmetry. Allowing this, the hole has a tendency to localize on one single oxygen, forming a dipole moment with the Li. However, our results alone cannot distinguish between these two cases.

ACKNOWLEDGMENTS

This investigation was supported by the Netherlands Foundation for Chemical Research (SON) and the Neth-

erlands Foundation for Fundamental Research on Matter (FOM) with financial support from the Netherlands Organization for the Advancement of Pure Research (NWO) and the Committee for the European Development of Science and Technology (CODEST) program.

-
- ¹N. F. Mott, Proc. Phys. Soc. London, Sec. A **62**, 416 (1949).
²J. Hubbard, Proc. R. Soc. London, Sec. A **277**, 237 (1964); **281**, 401 (1964).
³J. M. McKay and V. E. Heinrich, Phys. Rev. Lett. **53**, 2343 (1984).
⁴G. A. Sawatzky and J. W. Allen, Phys. Rev. Lett. **53**, 2339 (1984).
⁵J. G. Bednorz and K. A. Müller, Z. Phys. B **64**, 189 (1986).
⁶See, for a review, A. J. Bosman and A. J. van Daal, Adv. Phys. **19**, 1 (1970).
⁷J. B. Goodenough, D. G. Wickham, and W. J. Croft, J. Phys. Chem. Solids **5**, 107 (1958).
⁸K. Terakura, T. Oguchi, A. R. Williams, and J. Kuebler, Phys. Rev. B **30**, 4734 (1984).
⁹A. Fujimori and F. Minami, Phys. Rev. B **30**, 957 (1984).
¹⁰S.-J. Oh, J. W. Allen, I. Lindau, and J. C. Mikkelsen, Phys. Rev. B **26**, 4845 (1982).
¹¹P. Kuiper, G. Kruijzinga, J. Ghijsen, G. A. Sawatzky, and H. Verweij, Phys. Rev. Lett. **62**, 221 (1989).
¹²W. Brogner, H. Bade, and W. Klemm, Z. Anorg. Allg. Chem. **333**, 188 (1964).
¹³H. P. Rooksby, Acta Crystallogr. **1**, 226 (1948).
¹⁴J. M. McKay and V. E. Heinrich, Phys. Rev. B **32**, 6764 (1985).
¹⁵S. Hufner and G. K. Wertheim, Phys. Rev. B **8**, 4857 (1973).
¹⁶J. Zaanen, C. Westra, and G. A. Sawatzky, Phys. Rev. B **33**, 8060 (1986).
¹⁷G. van der Laan, C. Westra, C. Haas, and G. A. Sawatzky, Phys. Rev. B **23**, 4369 (1981).
¹⁸H. Eskes and G. A. Sawatzky, Phys. Rev. B **43**, 119 (1991).
¹⁹J. J. Yeh and I. Lindau, At. Data Nucl. Data Tables **32**, 1 (1985).
²⁰P. Kuiper, J. van Elp, G. A. Sawatzky, A. Fujimori, S. Hosoya, and D. M. de Leeuw, Phys. Rev. B **44**, 4570 (1991).
²¹R. Lof *et al.* (unpublished).
²²M. Khairy, P. Odier, and J. Choisnet, J. Phys. (Paris) Colloq. **C1-47**, 831 (1986).
²³C. P. J. Soethout, G. P. J. Geelen, and D. M. de Leeuw (unpublished).
²⁴J. C. Slater and G. F. Koster, Phys. Rev. **94**, 1498 (1954).
²⁵L. F. Mattheiss, Phys. Rev. B **5**, 290 (1972).
²⁶Z.-X. Shen, C. K. Shih, O. Jepsen, W. E. Spicer, I. Lindau, and J. W. Allen, Phys. Rev. Lett. **64**, 2442 (1990).
²⁷J. Meng, P. Jena, and J. M. Vail, J. Phys. Condens. Matter **2**, 10371 (1990).
²⁸T. van Oosten (private communication).
²⁹P. Kuiper, Ph.D. thesis, University of Groningen, 1990.
³⁰J. Zaanen, Ph.D. thesis, University of Groningen, 1986.
³¹J. S. Griffith, *The Theory of Transition Metal Ions* (Cambridge University Press, Cambridge, 1961).
³²W. A. Harrison, *Electronic Structure and the Properties of Solids* (Freeman, San Francisco, 1980).
³³D. E. Eastman and J. L. Freeouf, Phys. Rev. Lett. **34**, 395 (1975).
³⁴R. Newman and R. M. Chrenko, Phys. Rev. **114**, 1507 (1959).
³⁵J. Zaanen, G. A. Sawatzky, and J. W. Allen, Phys. Rev. Lett. **55**, 418 (1985).
³⁶J. van Elp, J. L. Wieland, H. Eskes, P. Kuiper, G. A. Sawatzky, F. M. F. de Groot, M. Abbate, and T. S. Turner, Phys. Rev. B **44**, 6090 (1991); see, in particular, Sec. 3.